UvA-DARE (Digital Academic Repository)

Continued cooling of the accretion-heated neutron star crust in the X-ray transient IGR J17480-2446 located in the globular cluster Terzan 5

Ootes, L.S.; Vats, S.; Page, D.; Wijnands, R.; Parikh, A.S.; Degenaar, N.; Wijngaarden, M.J.P.; Altamirano, D.; Bahramian, A.; Cackett, E.M.; Heinke, C.O.; Homan, J.; Miller, J.M.

Link to publication

Citation for published version (APA):

Continued cooling of the accretion-heated neutron star crust in the X-ray transient IGR J17480–2446 located in the globular cluster Terzan 5

L. S. Ootes,[1]★ S. Vats ,[1] D. Page,[2] R. Wijnands,[1] A. S. Parikh,[1] N. Degenaar,[1]
M. J. P. Wijngaarden ,[3] D. Altamirano,[4] A. Bahramian ,[5] E. M. Cackett ,[6]
C. O. Heinke ,[7] J. Homan[8,9] and J. M. Miller[10]

[1]*Anton Pannekoek Institute for Astronomy, University of Amsterdam, Science Park 904, NL-1098 XH Amsterdam, the Netherlands*
[2]*Instituto de Astronomía, Universidad Nacional Autónoma de Mex´ico, Mexico D.F. 04510, Mexico*
[3]*Mathematical Sciences, University of Southampton, SO17 1BJ, Southampton, UK*
[4]*Physics and Astronomy, University of Southampton, SO17 1BJ, Southampton, UK*
[5]*Department of Physics and Astronomy, Michigan State University, East Lansing, MI 48824, USA*
[6]*Department of Physics and Astronomy, Wayne State University, 666 W. Hancock St. Detroit, MI 48201, USA*
[7]*Department of Physics, University of Alberta, CCIS 4-183, Edmonton, AB T6G 2E1, Canada*
[8]*Eureka Scientific Inc., 2452 Delmer Street, Oakland, CA 94602, USA*
[9]*SRON, Netherlands Institute for Space Research, Sorbonnelaan 2, NL-3584 CA Utrecht, the Netherlands*
[10]*Department of Astronomy, University of Michigan, 1085 South University Ave., Ann Arbor, MI 48109, USA*

ABSTRACT

We present a new *Chandra* observation (performed in 2016 July) of the neutron star X-ray transient IGR J17480–2446, located in the globular cluster Terzan 5. We study the continued cooling of the neutron star crust in this system that was heated during the 2010 outburst of the source. This new observation was performed 2 yr after the last observation of IGR J17480–2446, hence, significantly extending the cooling baseline. We reanalysed all available *Chandra* observations of the source (but excluding observations during which one of the known transients in Terzan 5 was in outburst) and fitted the obtained cooling curve with our cooling code NSCOOL, which allows for much improved modelling than what was previously performed for the source. The data and our fit models indicate that the crust was still cooling ∼5.5 yr after the outburst ended. The neutron star crust has likely not reached crust-core thermal equilibrium yet, and further cooling is predicted (which can be confirmed with additional *Chandra* observations in >5 yr). Intriguingly, we find indications that the thermal conductivity might be relatively low in part of the crust compared to what has been inferred for other crust-cooling sources and tentatively suggest that this layer might be located around the neutron drip. The reason for this difference is unclear, but might be related to the fact that IGR J17480–2446 harbours a relatively slowly rotating neutron star (with a spin of 11 Hz) that has a relatively strong inferred surface magnetic field (10^{9-10} Gauss) compared to what is known or typically assumed for other cooling sources.

Key words: stars: neutron – X-rays: binaries – X-rays: individual: IGR J17480–2446.

1 INTRODUCTION

Low-mass X-ray binaries (LMXBs) harbouring neutron star primaries are excellent laboratories for studying the thermal evolution of accretion-heated neutron star crusts and, through such studies, they allow us to investigate the physical processes at work in the dense matter present in such crusts. As matter gets accreted from the (sub-)solar secondary (via Roche-lobe overflow) onto the surface of the neutron star, the newly accreted matter compresses the underlying material in the stellar crust. This leads to a series of exothermic reactions like electron captures, neutron emission, and, most energetically, density-driven nuclear fusion reactions (e.g. Haensel & Zdunik 1990, 2008; Steiner 2012) that cause heating of the neutron star crust and eventually the neutron star core (e.g. Brown, Bildsten & Rutledge 1998; Colpi et al. 2001). Most of the

★ E-mail: l.s.ootes@uva.nl

energy generated by these reactions is released deep in the crust (at a density of $\sim 10^{12-13}$ g cm^{-3}) and this process is therefore commonly referred to as the 'deep crustal heating' mechanism.

A few dozen neutron star LMXBs are persistently accreting sources so that the neutron star is typically outshone by the X-rays produced by the accretion process. However, many neutron star LMXBs systems are transients that only occasionally accrete matter during so-called outbursts (for a review on neutron star X-ray transients, see Campana et al. 1998). The duration of such outbursts can vary widely and can range anywhere from several days (e.g. Wijnands et al. 2009; Heinke et al. 2010; Mata Sánchez et al. 2017) to decades (e.g. Remillard 1999; Wijnands et al. 2001b; for reviews on the outburst behaviour of X-ray transients, we refer to Chen, Shrader & Livio 1997 and Yan & Yu 2015; for a review about the physical processes behind such outbursts, see Lasota 2001). During an outburst, the X-ray luminosities of transient neutron star LMXBs reach $L_X \sim 10^{35}$–10^{38} erg s^{-1}. Such accretion outbursts are followed by longer periods of quiescence. During this phase, they can still be detectable at X-ray luminosities of $L_X \sim 10^{31}$–10^{34} erg s^{-1}. This low level of the quiescent X-ray luminosity indicates that the accretion onto the neutron star is only active at a very low rate or has almost completely halted. In the latter case, if the neutron star is sufficiently hot, we are able to study the emission directly from the neutron star surface, from which the thermal state of the neutron star (both its crust and its core) can be inferred (for a review focusing on the observational results on this topic, see Wijnands, Degenaar & Page 2017).

During outburst, the energy released from the aforementioned reactions heats up the crust. If a sufficient amount of energy is released, the crust can be heated out of thermal equilibrium with the core. After the end of the outburst, the crust will cool until it is in equilibrium with the core again (e.g. Brown et al. 1998; Ushomirsky & Rutledge 2001; Rutledge et al. 2002). This cooling has been observed for about ten[1] systems (Wijnands et al. 2017) and such studies have led to new insights into the physical processes at work in the crust. The two highest impact conclusions from these studies are that the crust has a high thermal conductivity (Wijnands et al. 2002; Cackett et al. 2006; Shternin et al. 2007; Brown & Cumming 2009; while, before these studies, typically a much lower conductivity was expected; e.g. Schatz et al. 2001) and that, besides the deep crustal heating, there must be an additional source of heating present at much lower depths in the crust ($\rho \sim 10^9$ g cm^{-3}) in several of the studied sources (e.g. Brown & Cumming 2009; Degenaar, Brown & Wijnands 2011b; Homan et al. 2014; Waterhouse et al. 2016).[2] Currently the origin of this shallow heat source is not understood (this is typically referred to as the 'shallow heating problem'; for an in-depth discussion, see Deibel et al. 2015).

1.1 IGR J17480–2446

IGR J17480–2446 (here onwards J1748) is an LMXB that harbours an 11 Hz accreting X-ray pulsar primary, and a secondary that has an estimated mass of $\simeq 0.8$–1.0 M$_\odot$ (Strohmayer et al.
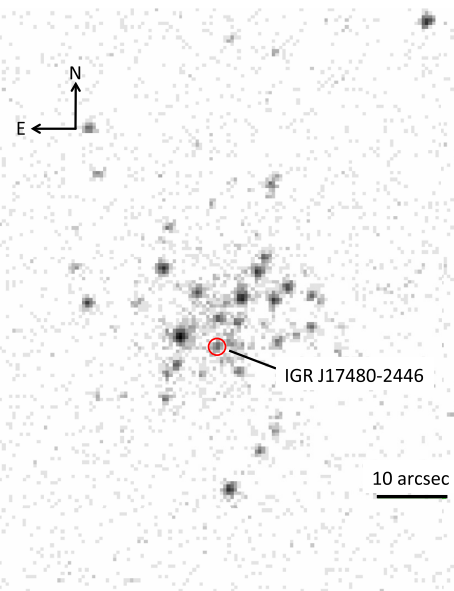

Figure 1. The *Chandra* 0.5–10 keV X-ray image of the globular cluster Terzan 5 obtained in 2016 July (ObsID-17779). IGR J17480–2446 is marked with a red circle.

2010; Strohmayer & Markwardt 2010; Patruno et al. 2012; Testa et al. 2012). The 11-Hz pulsations and the type-I X-ray bursts (Strohmayer & Markwardt 2010) observed from this source established the neutron star nature of the primary star. The source is located in the globular cluster Terzan 5 (Fig. 1) at a distance of $D \simeq 5.5$ kpc (Ortolani et al. 2007). J1748 exhibited an outburst of approximately two months in 2010[3] (Degenaar & Wijnands 2011b).

Before the 2010 outburst of J1748, Terzan 5 was the target of several *Chandra* observations during which no X-ray transient was active (Wijnands et al. 2005; Heinke et al. 2006b). Due to these observations, the pre-outburst quiescent counterpart of J1748 could be readily identified (Pooley et al. 2010), which serves as a proxy for the quiescent base level of this transient (and hence gives us a clear indication of the thermal state of the neutron star core in this system; Degenaar & Wijnands 2011a). After the accretion outburst of 2010, Degenaar & Wijnands (2011b) found (using a *Chandra* observation about two months after the end of this outburst) that the quiescent counterpart was significantly brighter than before this outburst. This strongly indicates that the crust of the neutron star in this source was heated considerably out of equilibrium with the core and this demonstrates that a short (only a few months) outburst can also cause significant heating of the crust (likely due to a strong shallow heat source present in these systems). Frequent monitoring of the source using about a dozen *Chandra* follow-up observations allowed the cooling of the neutron star crust to be studied (Degenaar et al. 2011a, 2013, 2015). Here we report on our continuous monitoring of the source using additional *Chandra* observations obtained in the summer of 2016 to further investigate its crust-cooling behaviour.

---

[1]For a few sources it needs to be confirmed that they are indeed crust-cooling sources as the observational results for them are not yet conclusive (see Wijnands et al. 2017).

[2]Several studies of thermonuclear explosions (so-called type-I X-ray bursts) on the surface of the neutron star also, independently, inferred the existence of this shallow heat source (e.g. Cumming et al. 2006; in 't Zand et al. 2012).

[3]Currently the 2010 outburst is the only outburst identified from J1748 although some of the old outburst activity observed from the direction of Terzan 5 may have been due to J1748 as well. However, this remains uncertain as the spatial resolutions of the earlier X-ray missions that observed these outbursts do not allow us to resolve sources in dense globular cluster cores (see also the discussion in Degenaar & Wijnands 2012).
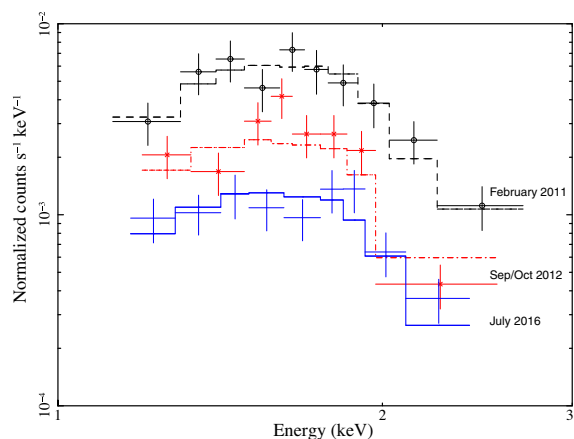
Figure 2. The X-ray spectra obtained during different epochs of our *Chandra* observations – the black points (○) represent the observation performed in 2011 February (ObsID 13225); the red points (×) represent the combined spectra obtained during the observations obtained in 2012 September and October (ObsIDs 14475 and 14476); the blue points (+) represent the combined spectra from the data obtained during the observations performed in 2016 July (ObsIDs 17779 and 18881). The individual best-fitting NSATMOS models for each spectrum are represented by similarly coloured lines (dashed for 2011 February, dash-dot-dash for 2012 September/October, solid lines for 2016 July). We only show three spectra, from the highest observed count rate (2011 February) to the lowest count rate (2016 July) detected so far, in order to avoid overcrowding in the figure.

2 OBSERVATIONS AND DATA ANALYSIS

We make use of archival *Chandra* observations[4] of Terzan 5 from 2003 to 2014 (this same set of observations was used by us before in our previous cooling studies of J1748; Degenaar et al. 2011a, 2013, 2015; Degenaar & Wijnands 2011b), combined with two new observations obtained in 2016 July (PI: Degenaar; see Table 1 for the log of the observations used in our study). The two observations from 2003 and 2009 were performed before the 2010 outburst of J1748 and were used to estimate the pre-outburst temperature of the neutron star, whereas the remaining observations were used to model the thermal evolution of the neutron star after its 2010 outburst. All observations were taken in the Faint, timed exposure mode, using the Advanced CCD Imaging Spectrometer S array (ACIS-S; Garmire et al. 2003), with a single frame exposure time of 3.0 s for all but six observations (ObsID 10059 – 1.6 s; ObsIDs 144[75-79] – 0.8 s). The cluster was positioned on the S3 chip.

We processed the level-1 event files using CIAO[5] 4.8, and using the latest calibration files (CALDB[6] 4.7.6). We created the level-2 event files with the chandra_repro script. To look for background flares, we created a background light curve for each observation in the energy range 0.5–10 keV using the dmextract routine. We found that during the observation performed in 2003 July (ObsID 3798) enhanced background flaring activity was present, showing more than 3σ excursions from the average background count rate. The original exposure time for this observation was ∼39.3 ks and the final exposure time after removal of the flares was ∼30.8 ks. The

Table 1. Log of the *Chandra* observations of J1748 used in our study.

Obs ID	Date	Exposure time (ks)	Count rate[1] (10^{-3} c s^{-1})
3798	2003 Jul 13/14	30.8[2]	0.87 ± 0.17
10059	2009 Jul 15/16	36.3	1.17 ± 0.18
13225	2011 Feb 17	29.7	6.18 ± 0.46
13252	2011 Apr 29	39.5	3.75 ± 0.31
13705	2011 Sep 5	13.9	3.37 ± 0.49
14339	2011 Sep 8	34.1	3.07 ± 0.30
13706	2012 May 13	46.5	2.61 ± 0.24
14475	2012 Sep 17/18	30.5	2.90 ± 0.31
14476	2012 Oct 28	28.6	2.40 ± 0.29
14477	2013 Feb 5	28.6	1.80 ± 0.25
14625	2013 Feb 22	49.2	2.12 ± 0.21
15615	2013 Feb 23	84.2	1.96 ± 0.15
14478	2013 Jul 16/17	28.6	2.16 ± 0.28
14479	2014 Jul 15	28.6	1.73 ± 0.25
16638	2014 Jul 17	71.6	1.82 ± 0.16
15750	2014 Jul 20	23.0	2.12 ± 0.30
17779	2016 Jul 13/14	68.8	1.31 ± 0.14
18881	2016 Jul 15/16	64.7	1.25 ± 0.14

Note. 1: Net (background subtracted) count rate (with 1σ errors) of J1748 in the energy range 0.5–10 keV. Typical (0.5–10 keV) background count rates during the observations are $(\sim2-8) \times 10^{-5}$ counts s^{-1}.
2: After removal of background flares.

remainder of the observations were free of background flares. We obtained the count rates for J1748 during each observation using dmextract (see Table 1). We used a source extraction region of radius 1 arsec centred on the brightest pixel of the source in the X-ray image. For the background extraction region, we made a selection on a source free part of the chip with a radius of 15 arcsec (this region was outside the field-of-view as shown in Fig. 1 and therefore not shown in that figure). We used these extraction regions to obtain the source and background spectra; the corresponding response files were generated using specextract.

For observations that were taken close to each other in time, we combined the spectra using the CIAO tool combine_spectra. The quiescence observations of 2003 and 2009 were also combined to increase the statistics of the pre-outburst spectrum. By doing this, we assume that the neutron star temperature was constant in the quiescent period preceding the 2010 outburst of the source. However, this appears to be a valid assumption since Degenaar & Wijnands (2011a) found that the two individual spectra were consistent with each other. We grouped the obtained spectra using grppha such that each bin contained a minimum of 15 photons, and then fitted (using χ^2 minimization) the 10 spectra we obtained in the 0.5–10 keV energy range using xspec.[7] We also fitted the data using the Cash statistics (Cash 1979, i.e. the way it is implemented in XSPEC so that it can also be used on background subtracted spectra; the so-called W-statistics) and we found that all data points had consistent temperatures between the two fit methods. In addition, the evolution of the temperature in time (see Section 3) was very similar. Not to complicate the paper, we only display the results obtained using the χ^2 statistics.

Table 2. The results obtained from our X-ray spectral analysis.

Epoch	MJD	$kT_{\rm eff}^{\infty}$ (eV)	F_X $(10^{-13}\,{\rm erg\,cm^{-2}\,s^{-1}})$	$F_{\rm bol}$ $(10^{-13}\,{\rm erg\,cm^{-2}\,s^{-1}})$	L_X $(10^{33}\,{\rm erg\,s^{-1}})$	$L_{\rm bol}$ $(10^{33}\,{\rm erg\,s^{-1}})$
2003/2009	52833.6/55027.7	77.7 ± 2.0	1.3 ± 0.2	1.8 ± 0.3	0.5 ± 0.1	0.7 ± 0.1
Feb 2011	55609.4	107.6 ± 1.8	6.0 ± 0.5	7.4 ± 0.6	2.2 ± 0.2	2.7 ± 0.2
Apr 2011	55680.7	98.2 ± 1.6	4.0 ± 0.4	5.1 ± 0.5	1.5 ± 0.1	1.8 ± 0.2
Sep 2011	55812.7	96.5 ± 1.6	3.7 ± 0.3	4.7 ± 0.4	1.3 ± 0.1	1.7 ± 0.2
May 2012	56060.8	90.9 ± 1.7	2.8 ± 0.3	3.7 ± 0.4	1.0 ± 0.1	1.3 ± 0.1
Sep/Oct 2012	56207.9	92.5 ± 1.6	3.1 ± 0.3	3.9 ± 0.4	1.1 ± 0.1	1.4 ± 0.1
Feb 2013	56336.8	89.0 ± 1.2	2.5 ± 0.2	3.3 ± 0.2	0.9 ± 0.1	1.2 ± 0.1
Jul 2013	56489.9	91.0 ± 2.3	2.8 ± 0.4	$3.7^{+0.6}_{-0.5}$	1.0 ± 0.2	1.3 ± 0.2
Jul 2014	56855.8	88.0 ± 1.5	2.4 ± 0.2	3.1 ± 0.3	0.9 ± 0.1	1.1 ± 0.1
Jul 2016	57583.6	84.8 ± 1.4	2.0 ± 0.2	2.7 ± 0.2	0.7 ± 0.1	1.0 ± 0.1

Notes. The combined NSATMOS fit using all spectra resulted in a neutral hydrogen column density, $N_{\rm H}$, of $2.96^{+0.12}_{-0.11} \times 10^{22}$ cm^{-2}. This value is slightly higher than what was reported by Degenaar et al. (2015), presumably because we are using the latest *Chandra* calibration files. The reduced χ^2 was 1.039 for 72 degrees of freedom. F_X and L_X are the unabsorbed X-ray flux and X-ray luminosity for 0.5–10 keV, and $F_{\rm bol}$ and $L_{\rm bol}$ are the unabsorbed bolometric flux and luminosity (using the 0.01–100 keV range as a proxy). The errors are at the 1σ confidence levels.

3 RESULTS

3.1 Observational results

We fitted all the spectra simultaneously using the neutron star atmosphere model (NSATMOS; Heinke et al. 2006a) in combination with TBABS to model the interstellar absorption (using the WILM abundances and the VERN cross-sections; Verner et al. 1996; Wilms, Allen & McCray 2000). In the NSATMOS model, we fixed the distance to 5.5 kpc (Ortolani et al. 2007), and initially set the neutron star mass and radius to $M = 1.4$ M$_\odot$ and $R = 10$ km, similar to what was used in our previous studies of this source (Degenaar & Wijnands 2011b; Degenaar et al. 2011b, 2013; see Section 3.1.1 for the effects on our results when using different assumed masses and radii). The neutron star was assumed to be emitting from its entire surface, which means that the normalization was set to unity. The hydrogen column density ($N_{\rm H}$) was assumed to remain constant through all the epochs. Hence, this parameter was tied between all the spectra. This model results in a satisfactory fit – $\chi^2/\nu = 1.039$ for 72 degrees of freedom (ν). The unabsorbed fluxes (0.5–10 keV) and corresponding X-ray luminosities were obtained by including the convolution model CFLUX. We also calculate the 0.01–100 keV fluxes and luminosities of the neutron star at each epoch, which can serve as good indicators for the bolometric fluxes[8] and luminosities during each observation. Finally, we obtained the effective neutron star temperature as seen by an observer at infinity, $kT_{\rm eff}^{\infty}$.[9] The neutron star temperatures, unabsorbed X-ray fluxes, and corresponding luminosities are shown in Table 2. The quoted uncertainties are at the 1σ level of confidence.

The 2010 outburst of J1748 started around MJD = 55 478 (Bordas et al. 2010; Linares & Altamirano 2010). The end of the outburst

[8]The cut-off energies (at both the low- and high-energy ends) of the NSATMOS model vary with the temperature. However, for the temperatures of interest in our paper, the model is defined down to at least 0.01 keV and the flux ignored below this energy is always <0.1 per cent of the total flux. At the upper bound, the model is defined up to at least several tens of keV (again depending on temperature) but with typically very low fluxes above this cut-off energy.

[9]$kT_{\rm eff}^{\infty} = kT_{\rm eff}/(1+z) = kT_{\rm eff} \cdot (1 - R_{\rm s}/R)^{1/2}$. Here, k is the Boltzmann constant. For our assumed neutron star of radius $R = 10$ km and mass $M = 1.4$ M$_\odot$, the gravitational redshift $(1+z) = 1.31$. With $R_{\rm s} = 2GM/c^2$ the Schwarzschild radius, G the gravitational constant, and c the speed of light.
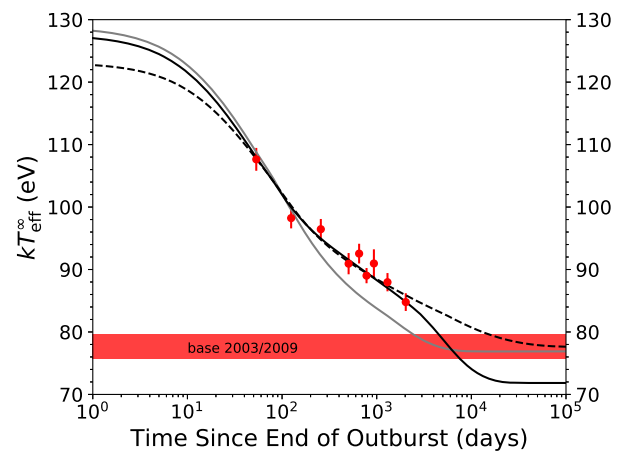

Figure 3. Observed cooling (red points) and exemplary cooling curves calculated using our NSCool code, for assumed mass $M = 1.4$ M$_\odot$ and radius $R = 10$ km. The black solid curve serves as an example for model 1. This curve is not forced back to the observed pre-outburst base level (red horizontal band), and we assumed for this curve $Q_{\rm imp}^{(2)} = 550$, and $Q_{\rm imp} = 25$ for the shallower ($Q_{\rm imp}^{(1)}$) and deeper ($Q_{\rm imp}^{(3,4,5)}$) impurity zones in the crust. The increased impurity factor delays the cooling after >100 d. The effect is shown by the grey curve, which shows a model in which the same parameters are assumed as for the solid black curve, except $Q_{\rm imp}^{(2)}$, which is also set to 25. Note that this curve is not forced to return the pre-outburst base level, the overlap of the grey curve with the red horizontal band is coincidental. The black dashed curve is an example curve for model 2, which is forced to cool down to the 2003/2009 base level.

was not observed because the source was in a Sun-constrained window around the time J1748 returned to quiescence. Degenaar & Wijnands (2011b) estimated the end of the outburst (and thus the starting date of the cooling phase) to be at $t_0 = 55\,556$. Using this starting date for the cooling phase, we could construct the cooling curve as shown in Fig. 3. Clearly, the source cooled significantly over the course of ~5.5 yr; from ~108 eV at the time of the first crust-cooling observation (in 2011 February) to ~85 eV during our new observations (2016 July). The same trend was reported by Degenaar et al. (2015), but we have extended the curve further using our new data. The new data point has a lower temperature compared to the previous point (obtained in 2014 July; see Table 2) demonstrating that, at that time, the crust was not in equilibrium yet with the core.

It should be emphasized though that the last two data points in Fig. 3 (corresponding to the 2014 July and 2016 July observations) have measured temperatures that are almost consistent with each other. However, the temperature decrease is supported by the fact that the source count rates (see Table 1) also decreased significantly between the corresponding observations. Moreover, when combining the 2014 July data (Obs IDs: 14479, 16638, 15750) together as well as the 2016 July data (Obs IDs: 17779 and 18881), we obtain a source count rate for these combinations of observations of $1.84 \pm 0.12 \times 10^{-3}$ counts s^{-1} and $1.30 \pm 0.10 \times 10^{-3}$ counts s^{-1}, respectively. Therefore, the count rate decrease is significant at the $\sim 3.4\sigma$ level and hence we consider the observed decrease in temperature robust. This strongly indicates that the crust has cooled further and that it was not yet back in equilibrium with the core in 2014 July. We note that this can be confirmed with future *Chandra* observations of the source.

It is also clear from Fig. 3 that the source has not yet reached the same temperature as what was observed before the 2010 outburst. However, it is unclear if the source should indeed reach the same level or if it could level off at a higher temperature. These two possibilities will be investigated further in the next section (Section 3.2) in which we model the observed cooling curve with our NSCool cooling code.

3.1.1 Variation in mass and radius

Initially, we assumed a neutron star mass $M = 1.4\,M_\odot$ and radius $R = 10$ km for our spectral fits, consistent with previous observational analysis. Under the assumptions made in our NSCool code (see Section 3.2), such a neutron star has a crust that is ~ 800 metres thick and a surface gravity $g_s = 2.43 \times 10^{14}$ cm s^{-2}. However, the crustal thickness can differ significantly depending on the mass and radius of the star; more compact stars (i.e. higher surface gravity) have smaller crust radii and vice versa. This can affect the results when trying to constrain the crustal parameters. But, the assumed mass and radius also affect the obtained temperatures from spectral fitting, and hence for consistency the assumed mass and radius should be the same for the spectral fits and NSCool models.

To be able to have the mass and radius as free parameters in our simulations, we reanalysed all the spectral data for nine different combinations of mass and radius ($M = [1.0, 1.4, 1.8]\,M_\odot$, and $R = [9, 12, 15]$ km), resulting in surface gravities $g_s = (0.66–4.61) \times 10^{14}$ cm s^{-2} (crust thickness $\Delta R \sim 0.4–2.9$ km, where the thickest crust corresponds to the lowest surface gravity; see Table A2). The results of the spectral analysis for different $M - R$ combinations are presented in Table A1 of Appendix A. The results show that the temperatures vary ~ 15 per cent at most over the range of $M - R$ combinations. Fig. A1 shows the surfaces in $M - R$ space formed by the obtained temperatures for the first and last observations.

3.2 Modelling the thermal evolution with NSCool

We modelled the temperature evolution of the neutron star crust in J1748 during outburst and in quiescence using our thermal evolution code NSCool (Page & Reddy 2013; Page 2016; Ootes et al. 2016, 2018). During outburst, the neutron star crust is heated out of thermal equilibrium with the core by the deep crustal heating processes that, in our model, are assumed to be directly correlated with the rate of mass accretion onto the neutron star. We apply the deep crustal heating model from table A.3 of Haensel & Zdunik (2008), which assumes an initial composition of pure ^{56}Fe below

the layer of accreted matter that has been processed by X-ray bursts, and results in a total heat release of 1.93 MeV per accreted nucleon. However, as discussed in Section 1, it has been found from previous studies of several of the other crust-cooling sources that a second heating process of unknown origin must be active during the outburst at shallow depths (see e.g. Brown & Cumming 2009). The shallow heating properties (its strength and depth) have been found to differ significantly between sources and even between different outbursts of the same source (e.g. Deibel et al. 2015; Parikh et al. 2017; Ootes et al. 2018). In our model, we assume it to be directly related to the accretion rate as well, although the validity of this assumption is currently unclear (see e.g. the discussion about this in Ootes et al. 2018, but also the recent results of Parikh et al. 2019).

To model the temperature evolution of the crust during outburst, we used the time-dependent accretion rate method as described in Ootes et al. (2016). The accretion rate of J1748 was determined from the 2–20 keV MAXI monitoring data of the source (Matsuoka et al. 2009).[10] For the accretion rate calculations, it is required to convert the count rates to bolometric fluxes. We used a conversion factor of 1.29×10^{-8} erg cm^{-2} count^{-1} and again assumed a distance of 5.5 kpc to be consistent with the spectral fits. This conversion factor was obtained from the bolometric luminosities reported by Papitto et al. (2012).[11] For each reported observation, the bolometric luminosity is converted back to bolometric flux, which is then compared to the MAXI count rates observed on the same day to calculate a conversion factor. The final conversion factor is obtained by averaging the conversion factors of the individual daily-averaged MAXI observations. The average outburst accretion rate that we find with this method is $\langle \dot{M} \rangle = 0.11\,\dot{M}_{Edd}$ (where $\dot{M}_{Edd} = 1.5 \times 10^{18}$ g s^{-1} is the Eddington accretion rate), which is consistent with the value estimated by Degenaar & Wijnands (2011a).

The observed temperature evolution during the crust cooling phase depends on the heating during the accretion outburst, the properties of the crust, and the temperature of the core. The amount of heating depends on the mass accretion rate and the strength (Q_{sh}) and depth (ρ_{sh}) of the shallow heating mechanism. For other sources the amount of shallow heating is typically found to be $Q_{sh} = 0–2$ MeV nucleon^{-1} (see e.g. Degenaar et al. 2015 and references therein, and Merritt et al. 2016; Ootes et al. 2018; Parikh et al. 2018, for more recent results), although at least one source needs significantly more shallow heat during one outburst ($Q_{sh} = 6–17$ MeV nucleon^{-1}; Deibel et al. 2015; Parikh et al. 2017).

The parameters affecting the thermal conductivity (and thus the temperature evolution) are the composition of the envelope (the region with $\rho < 10^8$ g cm^{-3}, which acts as a heat blanket), parametrized by the amount of light elements in this layer, and the level of impurity in the solid part of the crust (set by the impurity parameter Q_{imp}). The envelope has a higher thermal conductivity if it consists of more light elements, which results in a higher surface temperature for the same internal temperature (i.e. the temperature below the envelope). A larger impurity factor decreases the thermal conductivity of the crust due to electron-impurity scattering. Within

---

[10] The MAXI light curve of J1748 can be found at http://maxi.riken.jp/star_data/J1748-248/J1748-248.html and is also shown in fig. 1 of Degenaar & Wijnands (2011b).

[11] Papitto et al. (2012) reported on the 0.05–150 keV luminosities that are reasonably accurate estimates for the bolometric ones. They quoted the luminosities for an assumed distance of 5.9 kpc so we converted them to 5.5 kpc (which we use in our work).

NSCOOL, one can define multiple density regions with different impurity factors. Typically, the impurity parameter throughout the crust is found to be $Q_{\rm imp} \sim 1\text{--}10$ (e.g. Brown & Cumming 2009; Cumming et al. 2017) from the modelling of observed cooling curves of several sources, although the impurity of the pasta layer (the innermost crust layer) might be larger (e.g. Horowitz et al. 2015; Deibel et al. 2017).

The specific heat of the crust depends on the presence of neutron superfluidity in the inner crust. If the dripped neutrons form a superfluid, they do not contribute to the neutron specific heat, hence reducing the total crust specific heat. The core temperature (parametrized by the gravitationally redshifted core temperature before the onset of accretion, $\widetilde{T}_0$) sets the equilibrium temperature between the crust and the core and thus affects the base level of the cooling curve. The assumed mass and radius set the surface gravity, and with that the thickness of the crust.

3.2.1 Exploring the parameter space with the Markov chain Monte Carlo method

The free parameters in our model are numerous (compared to the number of data points) and moreover degenerate, which makes it difficult to constrain the parameters of our model using simple fitting methods. Therefore, we did a full exploration of the parameter space in search for the parameters that best reproduce the data. This is done by using NSCOOL together with our recently developed Markov chain Monte Carlo (MCMC) driver MXMX (see Page, Ootes & Degenaar 2019, for full details), which allows us to consider a larger number of parameters.[12]

MXMX is inspired from emcee (Foreman-Mackey et al. 2013), but written in Fortran and designed for maximum efficiency when coupled with NSCOOL. Here we use it with 100 walkers and run it for 40 thousand steps (with auto-correlation times typically of the order of 50–250). In total, we thus run more than four million cooling curves and eliminate an initial set of points ('burn-in points') to keep only the part of the chain after convergence (see Fig. B2). In all cases the number of points we use in our statistics is at least a hundred times more than the integrated auto-correlation time (Sokal 1997) of the chain. The MCMC simulations show the χ^2 distribution to have a second local minimum, i.e. the distribution is bi-modal, as displayed in Fig. B1, but with a large (>75) χ^2, which requires the use of tempered chains in our simulations. Moreover, the time to reach convergence is long, which we determine by verifying that the χ^2 distribution becomes stationary, as illustrated in Fig. B2.

We run two different models. The first model (model 1) fits the nine data points observed after the 2010 outburst ended. Since it is not clear from these observations whether the surface temperature of the neutron star has levelled off already (which would indicate that the source is back in crust–core thermal equilibrium) the base level for this model is free. However, the source was also observed in quiescence before the start of its 2010 outburst. From observations taken in 2003 and 2009, a quiescence surface temperature of $77.7 \pm 2.0\,\text{eV}$ was measured (assuming $M = 1.4\,\text{M}_\odot$ and $R = 10$ km; see Table 2). Assuming that the source was in thermal equilibrium at the time of these pre-outburst observations, J1748 can be expected to eventually cool to this base level. Hence in the second model, we tested this scenario by forcing the calculated cooling curve to return

to the 2003/2009 base level (the red horizontal band in Fig. 3), by adding an additional point to the quiescence observations. This point, with a temperature equal to the one determined from the 2003/2009 observations, was set at a time of 10^5 d after the end of the outburst, such that we leave the time at which the source returns to the pre-outburst base level (which is typically $\sim 10^{3\text{--}4}$ d into quiescence) free. This requirement is not added to model 1, because the source may cool down to a new base level. Even though the core temperature T_0 is not expected to change considerably over the time of the 2010 outburst, the base level after the outburst can still be significantly different due to a change in envelope composition compared to that at the time of the pre-outburst measurement.

Our MCMC parameters, and their *prior* distributions, are as follows:

(i) The mass M, with a uniform prior distribution between $1.0\,\text{M}_\odot$ and $1.8\,\text{M}_\odot$.

(ii) The radius R, with a uniform prior distribution between 9.0 and 15.0 km.

(iii) Initial (redshifted) core temperature ($\widetilde{T}_0$), with a $\log \widetilde{T}_0$ prior distribution chosen as uniform between 7 and 9.[13]

(iv) The impurity parameter ($Q_{\rm imp}$) within the crust is divided into five regions according to density: $Q_{\rm imp}^{(1)}$ for the region $\rho < 10^{11}$ g cm^{-3}, $Q_{\rm imp}^{(2)}$ for $\rho = 10^{11-12}$ g cm^{-3}, $Q_{\rm imp}^{(3)}$ for $\rho = 10^{12-13}$ g cm^{-3}, $Q_{\rm imp}^{(4)}$ for $\rho = 10^{13-14}$ g cm^{-3}, and $Q_{\rm imp}^{(5)}$ for $\rho > 10^{14}$ g cm^{-3}. All $Q_{\rm imp}^{(i)}$ have prior distributions uniform between 0 and 1500. The upper bound allows for the possibility of highly amorphous crust structures.

(v) The column densities of Helium ($y_{\rm He}$) and Carbon ($y_{\rm C}$) in the envelope, with values chosen from uniform distributions between 0 and 10 for $\log y_{\rm He}$ and between 0 and 12 for $\log y_{\rm C}$, both in units of g cm^{-2}.

(vi) Shallow heating strength $Q_{\rm sh}$, with uniform prior distribution between 0 and 5 MeV per accreted nucleon.

(vii) The minimum density $\rho_{\rm sh}^{\rm min}$ and maximum density $\rho_{\rm sh}^{\rm max}$ of the shallow heating layer where the energy $Q_{\rm sh}$ is injected. Values of $\log \rho_{\rm sh}^{\rm min}$ and $\log \rho_{\rm sh}^{\rm max}$ are chosen from a uniform distribution between 8 and $\log \rho_{\rm cc}$, in units of g cm^{-3}. Here, $\rho_{\rm cc}$ is the crust-core transition density, which we fix at 1.5×10^{14} g cm^{-3}. Within the layer ranging between densities $\rho_{\rm sh}^{\rm min}$ and $\rho_{\rm sh}^{\rm max}$, the $Q_{\rm sh}$ heat is uniformly injected per unit volume.

(viii) The fraction ($a_{\rm entr}$) of dripped neutrons in the inner crust which are entrained by the nuclei in their thermal motion, uniformly distributed between 0 and 1. This parameter increases the nuclei effective mass and affects their specific heat (Chamel, Page & Reddy 2013) as well as the electron-phonon scattering rate a low temperature (but the latter is actually ineffective here because of impurity scattering that dominates unless $Q_{\rm imp}$ is very small). In a similar fashion as $Q_{\rm imp}$, $a_{\rm entr}$ should be considered as density dependent, but in this study we adopt a single value in the whole inner crust and, as we will see, its effect is negligible.

(ix) The density range, $\rho_{\rm SF}^{\rm min} - \rho_{\rm SF}^{\rm max}$, in which dripped neutrons in the inner crust are assumed to be superfluid with a high critical temperature, $T_c = 10^{10}$ K, while they are normal below and above this range. The values of $\rho_{\rm SF}^{\rm min}$ and $\rho_{\rm SF}^{\rm max}$ are constrained to be larger

---

[12]MCMC with Bayesian statistics works even if the number of parameters is larger than the number of data points (as is the case in our studies) but will likely then show that most of these parameters are unconstrained.
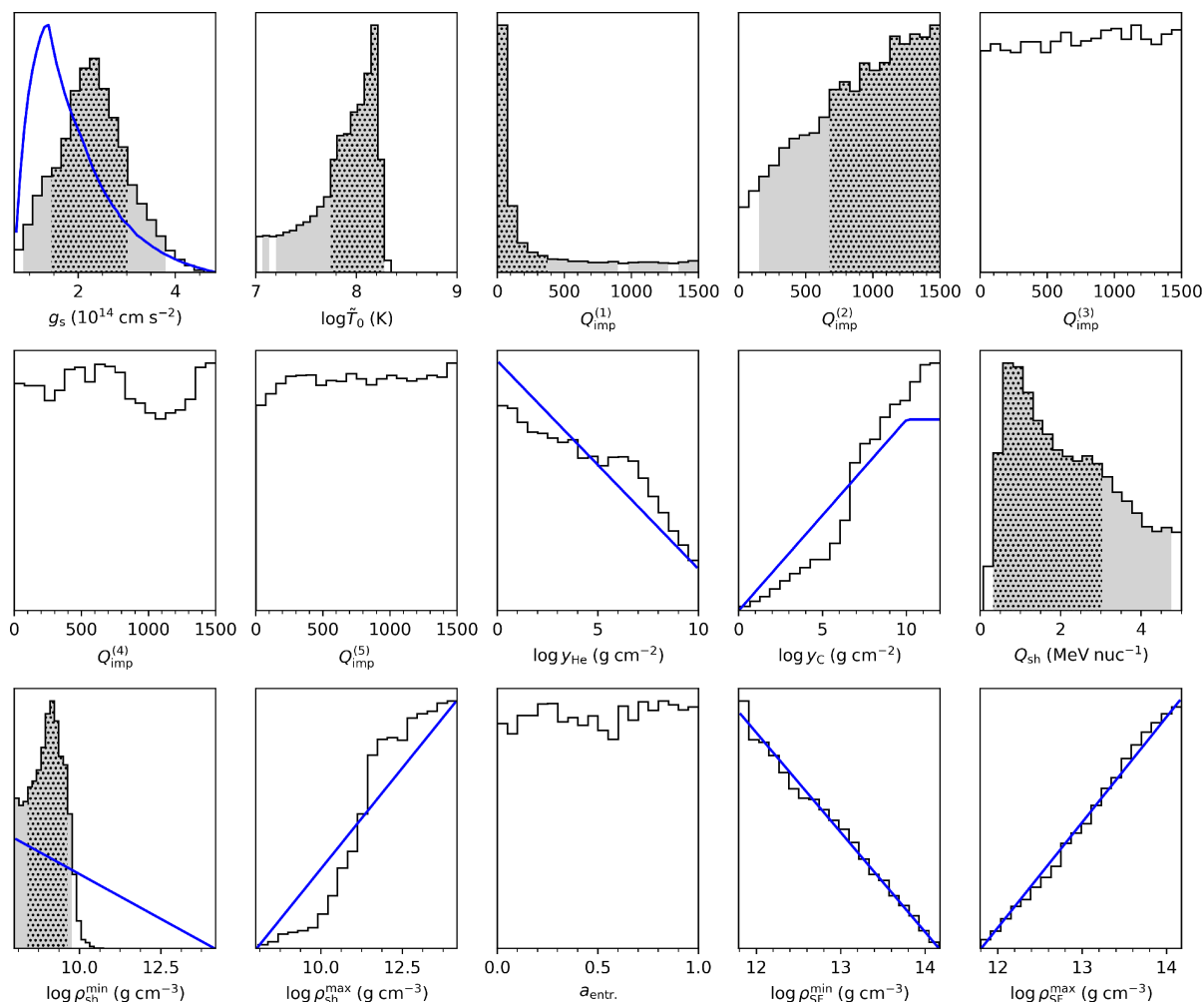
[13]Due to general relativistic effects, in a thermally relaxed state the local temperature T is *not* uniform in the stellar interior, but it is rather the redshifted temperature $\widetilde{T} \equiv e^\phi T$ which is uniform, the redshift factor e^ϕ being given by the time part of the metric g_{00} through $g_{00} = e^{2\phi}$ (see e.g. Page et al. 2004).

Figure 4. Histograms of the posterior probability distributions of our MCMC parameters for model 1. We show here g_s instead of M and R, and plot for the parameters that have non-uniform prior distributions (i.e. g_s, $\log y_{He}$, $\log y_C$, $\log \rho_{sh}^{min}$, $\log \rho_{sh}^{max}$, $\log \rho_{SF}^{min}$, and $\log \rho_{SF}^{max}$) their prior distribution in blue for comparison. The grey-filled bins indicate the region of decreasing likelihood that makes up 95 per cent of the area under the distribution and similarly, the dot-filled bins indicate the region that makes up 68 per cent of the total area. These areas are omitted if the posterior distribution is (nearly) identical to the prior distribution, indicating that the parameter cannot be constrained from this model. Vertical scale is arbitrary. See the text for details.

than the neutron drip density $\rho_{drip} \simeq 7 \times 10^{11}$ g cm^{-3} and smaller than ρ_{cc}. Both the $\log \rho_{SF}^{min}$ and $\log \rho_{SF}^{max}$ values are chosen from uniform distributions within their allowed ranges. The effect of superfluidity is to strongly suppress the neutron specific heat within this density range.

Our M and R parameters are chosen within the range of our $M - R$ grid assumed for the data analysis. As mentioned before, one should, for consistency, assume the same mass and radius for the model simulation as was assumed for the analysis of the observations. Therefore, for each point in our MCMC simulation, we interpolate the temperatures from Table A1 in accordance with the M and R assumed in that calculated cooling curve.

Although all values are chosen from uniform distributions, we additionally require all values to be physical. This means that we require $y_C > y_{He}$, $\rho_{sh}^{max} > \rho_{SF}^{min}$, and $\rho_{SF}^{max} > \rho_{SF}^{min}$. This leads to non-uniform prior distributions for these six parameters (see Fig. 4 for the prior distributions of the parameters for which the prior is not uniform).

The total number of free parameters in these simulations is larger than the number of data points. However, each one of them

controls an important physical (heating rate, thermal conductivity, and specific heat) or geometrical (curst thickness through g_s by M and R) ingredient of our cooling simulations. Most of these parameters will be unconstrained by the data but instead of choosing *a priori* which ones are or are not important we prefer to keep maximum freedom and let the MCMC method guide us.

3.2.2 Model 1: free base level

The results of our MCMC run for model 1 are presented in Figs 4 and 5. Fig. 4 shows the posterior distributions of all parameters in our MCMC run (but with M and R converted to g_s). In Fig. 5 we present the 2D histograms of a selection of the parameters, which shows the relations between different parameters. In Fig. 3 we show the observed temperatures and some exemplary calculated cooling curves. The posterior distributions in Fig. 4 show that, as expected, only a few of our MCMC parameters are constrained and that even for those the allowed parameter ranges are large. Nevertheless, we describe here the posterior distributions in attempt to compare them with expected values.
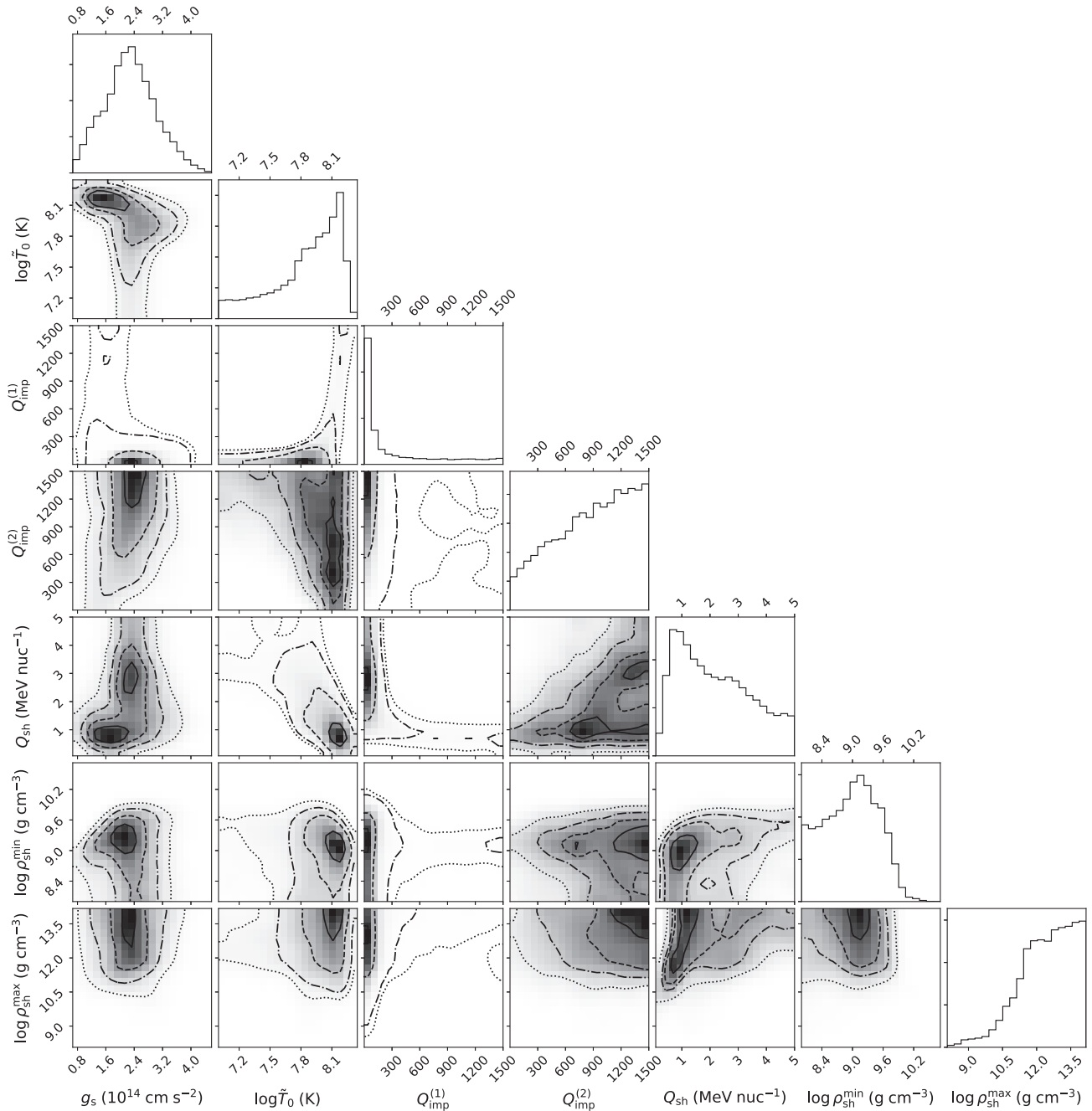
Figure 5. Results of our model 1 MCMC for selected parameters: g_s, $\tilde{T}_0$, $Q_{imp}^{(1)}$, and $Q_{imp}^{(2)}$ (i.e. the impurity factor for the outer two crust layers $\rho < 10^{11}$ and $\rho = 10^{11-12}$ g cm^{-3}), and shallow heating parameters (strength and depth). The solid, dashed, dashed-dotted, and dotted curves show, respectively, the 0.5σ, 1.0σ, 1.5σ, and 2.0σ levels in the 2D histograms.

The posterior distribution of the surface gravity peaks around ~ 2.3 cm s^{-2}. This peak includes the surface gravity of $g_s = 2.43$ cm s^{-2} that was assumed in our initial analysis of the observations (i.e. mass $M = 1.4$ M$_\odot$ and radius $R = 10$ km). However, the distribution also shows that only the most extreme surface gravities are outside the preferred range.

From our model 1, the core temperature cannot be constrained. The posterior distribution shows a preference for high core temperatures (with a peak around log $\tilde{T}_0 \sim 8.1$ K), but lower values are still allowed. Only the highest values (log $\tilde{T}_0 \gtrsim 8.3$ K) can be excluded based on this simulation.

The properties of the deepest layers of the crust remain unconstrained for this model as well, as the impurity parameter in these layers (layers 3–5, which coincide with densities $\rho > 10^{12}$ g cm^{-3}), as well as the parameters for the superfluidity in the inner crust, are found to have posterior distributions that are very close to the corresponding priors. Additionally, we do not obtain any constraints on the dripped neutron entrainment, a_{entr}, which only affects the specific heat in the deep inner crust. This indicates that this star has to evolve further in time for its surface temperature to be sensitive to the physics of the deep inner crust (see the discussion of this $T_{eff}(t)$ $- T(\rho)$ mapping in Brown & Cumming 2009). Furthermore, no

constraints on the envelope composition of J1748 can be obtained from model 1. The posterior distributions for $\log y_{He}$ and $\log y_C$ are close to the prior distributions.

On the other hand, the posterior distributions of the impurity parameter for the two outermost layers of the crust show a very interesting trend. Even though a precise value of $Q_{imp}^{(1)}$ and $Q_{imp}^{(2)}$ cannot be constrained from the posterior distributions in Fig. 4, the lowest values of the allowed range seem to be preferred for the impurity in the outermost region of the crust (impurity region 1; $\rho < 10^{11}\,\mathrm{g\,cm^{-3}}$, although it should be noted that the grey-shaded area in the panel for $Q_{imp}^{(1)}$ in Fig. 4 shows that larger values are not excluded), while in the second region of the crust, around the neutron drip density ($\rho = 10^{11-12}\,\mathrm{g\,cm^{-3}}$), the posterior distribution shows a preference for high values of the impurity parameter. The 95 per cent confidence range in the panel for $Q_{imp}^{(2)}$ in Fig. 4 shows a preference for values $Q_{imp}^{(2)} \gtrsim 150$. Such a value is $\gtrsim 10$ times larger than what has been found for other crust-cooling sources. The black curve in Fig. 3 represents a model with $Q_{imp}^{(2)} = 550$, while the value in the other layers is lower ($Q_{imp}^{(1,3,4,5)} = 25$). To show the effect of the high impurity layer for this particular curve, a grey curve is added to the figure that shows a cooling curve that assumes the same parameters as the black curve, but with a constant $Q_{imp} = 25$

throughout the crust. In Wijngaarden et al. (2018), we presented a preliminary model (using NSCOOL as well) of the thermal evolution of J1748, but without our newly added data point from 2016 July. In that work a different method was applied, which did not include the same free parameters. Nevertheless, we found a large impurity parameter for part of the crust in that work as well.

The shallow heating is modelled with three parameters. The posterior distribution of model 1 for the shallow heating strength peaks around ~ 1 MeV nucleon^{-1}, and shows that to fit the cooling data, at least some shallow heating is required. We find a preference for a minimum depth of the shallow heating around $\sim 10^9$ g cm^{-3} (and with an allowed range up to $\sim 10^{10}$ g cm^{-3}), in agreement with typical values found for other sources. The poster distribution for the maximum depth of the shallow heating layer allows for a large range of parameters, and shows that the shallow heating range may extend into the inner crust. However, our current observations do not allow us to constrain the inner crust yet. It is interesting to note that Fig. 5 shows that the highest values of the shallow heating strength ($Q_{sh} \gtrsim 3.5$ MeV nucleon^{-1}) are only allowed for large values of the maximum shallow heating depth ($\log \rho_{sh,\,max} \gtrsim 12$ g cm^{-3}), in which case most of the heat is deposited in the unprobed region.
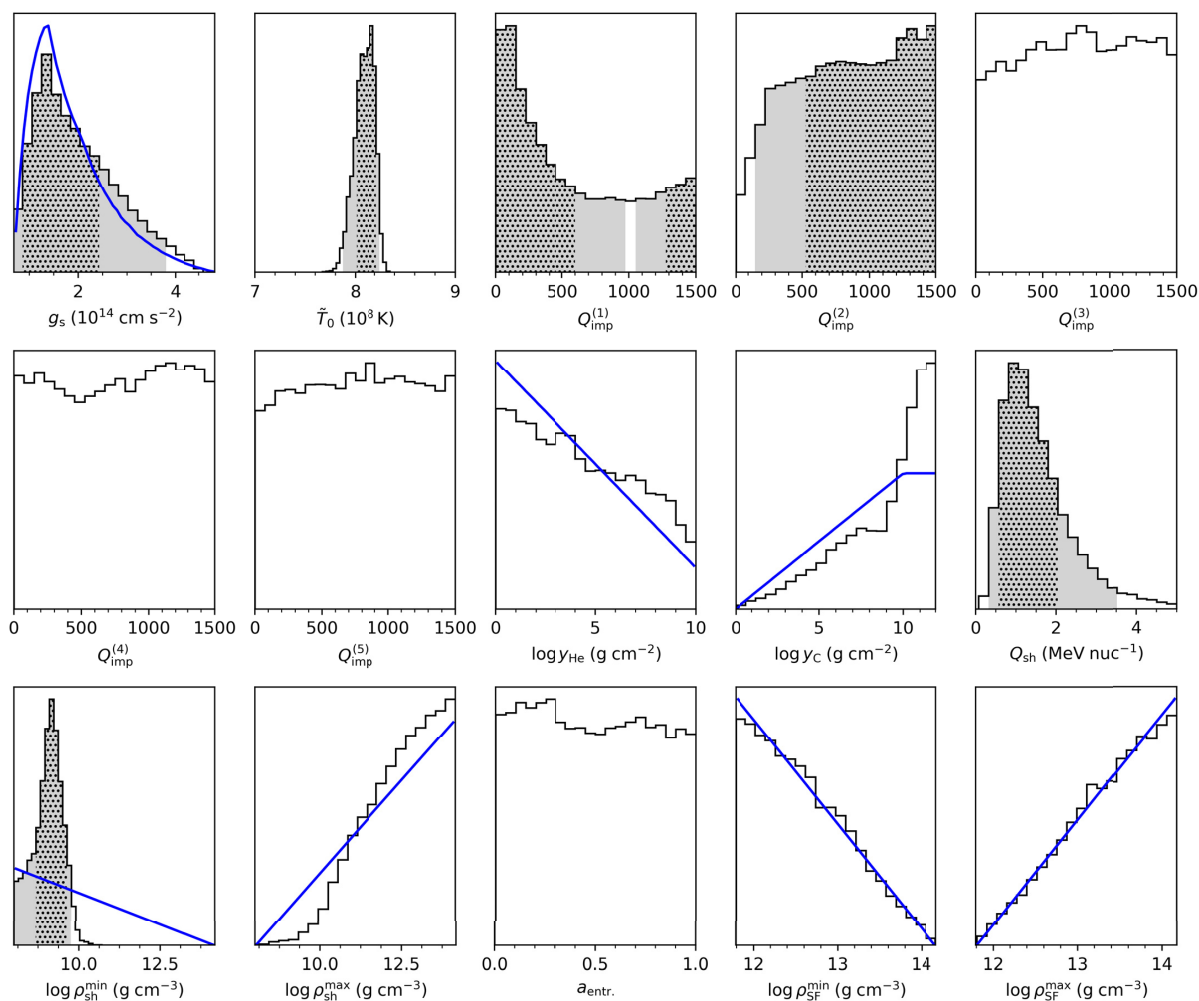

Figure 6. Same is Fig. 4, but for model 2 in which we force the source to cool down to the pre-outburst base level.
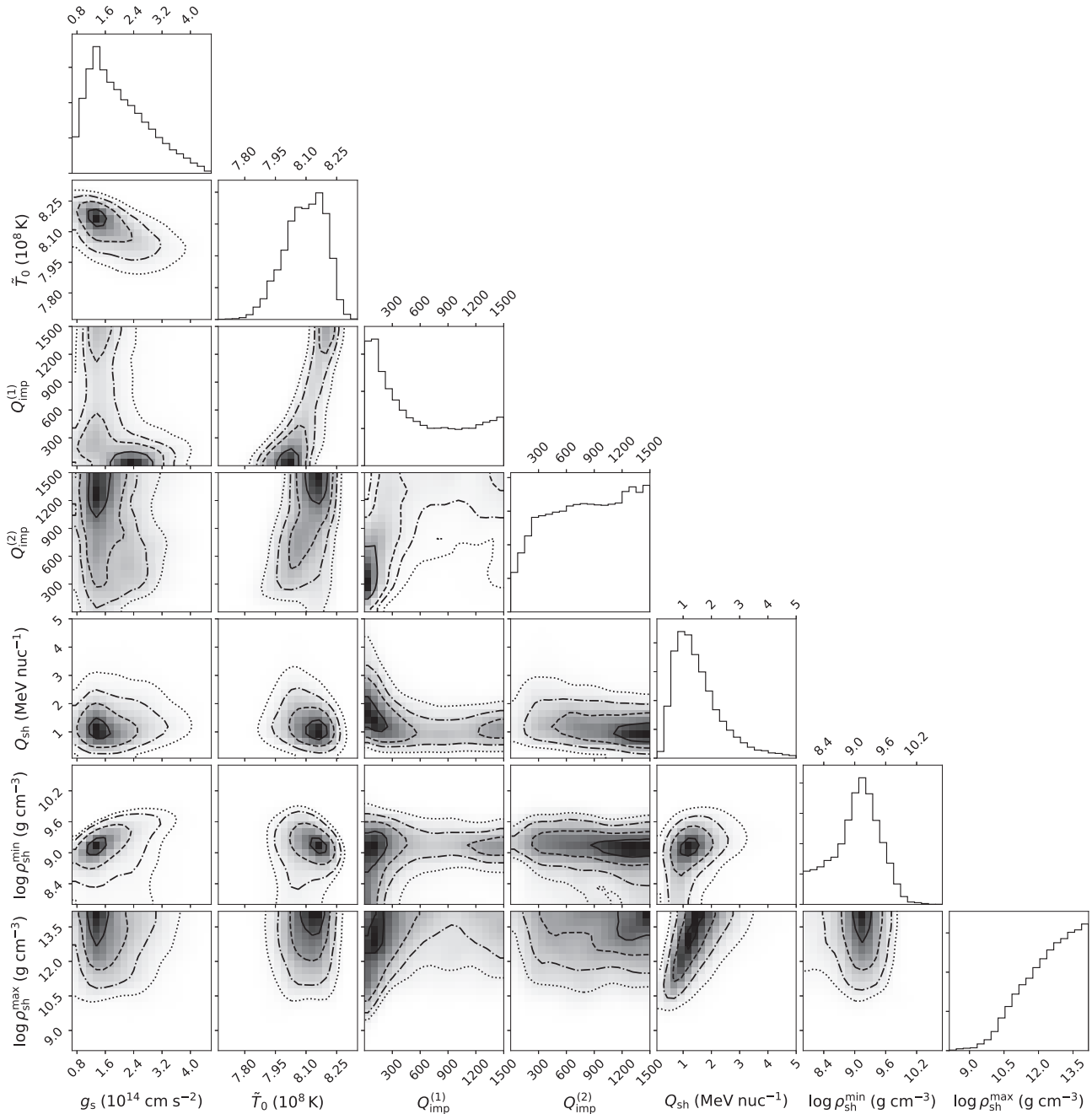
Figure 7. Results of model 2 for a selection of parameters. The solid, dashed, dashed-dotted, and dotted curves show, respectively, the 0.5σ, 1.0σ, 1.5σ, and 2.0σ levels in the 2D histograms.

3.2.3 Model 2: including the pre-outburst base level

In model 2, a hypothetical observation is added to the cooling data to force further cooling towards to pre-outburst base level. The time at which base level is reached is left free by adding this additional point at 10^5 d after the end of the outburst. The results are shown in Figs 6 and 7.

As expected, model 2 places more constraints on the core temperature than model 1. The posterior distribution shows again a peak around $\log \tilde{T}_0 \sim 8.1$ K, but the allowed range is much more constrained (the grey area comprises $\log \tilde{T}_0 \sim (7.85 - 8.25)$ K). The surface gravity and envelope composition are not constrained

for model 2, and hence no conclusions can be drawn on the values of these parameters for J1748.

The results for Q_{imp} and the envelope composition for model 2 are similar to those for model 1. As a consequence of the constraint on the core temperature, the impurity parameter for the outmost region of the crust $Q_{\mathrm{imp}}^{(1)}$ becomes less constrained compared to model 1 (see Fig. 7). We do find again that the impurity parameter in the second layer of the crust seems to prefer higher values ($Q_{\mathrm{imp}}^{(2)} \gtrsim 150$, from the grey area in Fig. 6) than found for other sources. When the source is forced to cool down to the pre-outburst base level, the posterior distribution for the shallow heating strength peaks stronger

around ∼1 MeV nucleon^{-1} compared to model 1, but the overall results for the shallow heating parameters are the same.

A constraint on the deepest region 5, where the nuclear pasta is expected to be found with a likely large Q_{imp}, would require several data points in the future as was recently exemplified by the last observation of MXB 1659-29 and its interpretation (Deibel et al. 2017). With multiple future observation, the base level as well as the time at which crust-core equilibrium is reached can be constrained, which would allow for constraints on the physics of the deep crust. These considerations also explain the absence of any constraints from model 2, on the one hand, on the dripped neutron entrainment, a_{entr}, which only affect specific heat in the deep inner crust and, on the other hand, on the crust superfluidity.

4 DISCUSSION

We used archival *Chandra* observations in conjunction with two new observations of Terzan 5 to study the thermal evolution of the neutron star in the X-ray transient IGR J17480–2446. Previous observations (up to the summer of 2014) showed that the neutron star crust in this system was significantly heated (i.e. out of thermal equilibrium with the core) during the 2010 outburst of the source and in the sub-sequent quiescent period the crust had cooled significantly (Degenaar & Wijnands 2011a,b; Degenaar et al. 2011a, 2013, 2015). The last observations reported previously were performed in 2014 July (Degenaar et al. 2015). In our paper we have presented new observations obtained 2 yr later, in 2016 July. With these new observations we span a post-outburst quiescent period of ∼5.5 yr allowing us to study the crust-cooling behaviour of this source in more detail. We fitted the source spectrum with an absorbed neutron star atmosphere model (i.e. NSATMOS) and found that the measured surface temperature was lower than the temperature observed during the 2014 July observations (see Table 2).

By modelling the thermal evolution of J1748 with our crust heating and cooling code NSCOOL (Page & Reddy 2013; Page 2016; Ootes et al. 2016, 2018), we have tried to constrain the crustal parameters of the neutron star in this source. We explore the full parameter space, using MCMC simulations. The source has been modelled before by Degenaar et al. (2011b, 2013), using a different code. In our current paper, we make use of more observations and use a more advanced code that takes into account accretion rate fluctuations based on the observed light curve (Ootes et al. 2016). Taking into account variations in accretion rate is especially important for short-duration transients such as J1748, because it is further off from a steady-state temperature profile during the outburst.

From our model 1 (which does not require the source to return to the 2003/2009 base level), we found that a shallow heating strength of the order of ∼1 MeV nucleon^{-1} is required to explain the temperature evolution in quiescence. The amount of shallow heating is not strongly constrained, but the model shows that at least some shallow heating is needed to reproduce the observations. For the depth of the shallow heating, we find a preference for a minimum depth around ∼10^9 g cm^{-3}, but full extent of the shallow heating region cannot be constrained from this model. Degenaar et al. (2013) fitted the temperature data obtained using the initial observations performed between 2011 and 2013 with $Q_{sh} = 1$ MeV nucleon^{-1}, similar to our results. On the other hand, Turlione, Aguilera & Pons (2015) found that the data were best fitted when an additional heat source of 3.8 MeV nucleon^{-1} was injected around a depth $\bar{\rho} = 4.3 \times 10^{11}$ g cm^{-3}. However, both studies used

different cooling models, which include different assumptions. For example, Turlione et al. (2015) fixed the boundary temperature T_b at the base of the envelope during the outburst. Their value of 3.8 MeV nucleon^{-1} is nevertheless within our posterior range (see Fig. 4).

The most peculiar result that we obtained from modelling the thermal evolution of this source is that we found indications that the impurity parameter of this neutron star might be higher in part of the crust compared to what has been found for other crust cooling sources. It should be emphasized that the results of model 1 do not provide strong constraints on the impurity parameter throughout the crust. Nevertheless, we found for J1748 that whereas the posterior distribution for the impurity in the outermost region of the crust showed a preference for values on the lower bound of our parameter range (which would be in accordance with other sources), our model suggested a large impurity ($Q_{imp}^{(2)} \gtrsim 150$, from the grey-shaded region in Fig. 4) in the second region of the crust ($\rho = 10^{11-12}$ g cm^{-3}, located around the neutron drip). However, the posterior distribution does not allow us to fully exclude the possibility of lower values for $Q_{imp}^{(2)}$.

Finally, our MCMC model 1 showed that core temperature prefers relative high values log $\tilde{T}_0 \sim 8.1$, but low values are not excluded. The envelope composition could not be constrained, and neither could the properties of the inner crust ($Q_{imp}^{(3,4,5)}$, superfluid range and dripped neutron entrainment) be probed. The main reason for this is that the base level of the cooling curve is still unknown. Our new observation showed that the observed surface temperature was lower than during previous observation, which indicates that the source is not yet in crust-core equilibrium and thus the base level might not be reached yet. Future observations that constrain the base level and the time at which this level is reached can constrain the parameters of the crust further, and can provide further insight in the potential high-impurity layer.

In model 1 we do not require the source to cool down to the pre-outburst base level. A change in base level after different outbursts can be explained by variation in envelope composition, determined by the burning processes during accretion. In a second MCMC simulation (model 2) we forced the source to cool down to the measured pre-outburst base level, but left the time at which this level was reached free. This provided constraints on the core temperature, and consequently affected the constraints on other parameters. These results highlight that in order to obtain stronger constraints on the crustal parameters of this source, J1748 needs to be observed in the future such that its base level and the time scale over which this level is reached can be determined.

Although it is clear that we cannot conclusively demonstrate that part of the crust in J1748 needs a high impurity parameter, our results are still suggestive of that and it is interesting to explore what could be the reason for this in this source. Recently, Lau et al. (2018) presented nuclear reaction network calculations for accreted neutron star crusts. Assuming various initial compositions (which depend on the thermonuclear burning processes taking place in the envelope), they calculated the reactions that a mass element undergoes as it is pushed deeper into the crust due to continued accretion. Based on the crust composition, they made a prediction for the impurity as function of density. They found that the impurity at $\rho \sim 10^9$ g cm^{-3} should have value of a few up to ∼80 (depending on the initial composition) and $Q_{imp} \sim 10$ (for all compositions) just after the neutron drip. As the authors point out, they have included the detailed scattering formalism by Roggero & Reddy (2016), which reduces the impurity by a factor of 2–4, and consequently the results found using cooling codes that do not include this formalism

(as is the case for our code) should be divided by this factor for comparison with the results from Lau et al. (2018). Although our findings do not directly compare with their results, variation in impurity throughout the crust does seem to improve the calculated cooling curves in order to reproduce the observations. However, a high-impurity region in the crust has not been found before for other sources, although in most cases the impurity is modelled to be constant throughout the crust (except for the deepest layer of the inner crust).

If it is indeed true that J1748 has a relatively low conductivity layer in the crust – potentially located around the neutron drip – compared to other sources, it is not clear what could cause this difference. Degenaar et al. (2013) suggested that the explanation for the difference in cooling behaviour between J1748 and the other sources might be related to several other unusual properties of the source. First of all, the source is a relatively slow rotating neutron star (with a spin of 11 Hz; Strohmayer & Markwardt 2010, see table 1 in Degenaar et al. 2015 for a comparison with other crust cooling sources). Although the neutron star spin has not been measured for all other crust-cooling sources, the sources that do have a measured spin all rotate significantly faster (>500 Hz; Smith, Morgan & Bradt 1997; Zhang et al. 1998; Wijnands, Strohmayer & Franco 2001a; Galloway et al. 2010). However, it is not clear how the spin could affect the heat conductivity and likely it cannot explain the difference in crustal conductivity between J1748 and the other sources (see the discussion in Degenaar et al. 2013 for more details).

Secondly, besides the slower spin rate, J1748 might also have a larger surface magnetic field strength (estimated to be 10^{9-10} Gauss; Cavecchi et al. 2011; Miller et al. 2011; Papitto et al. 2011, 2012) compared to the other sources (no strong constraints exist for these other sources but typically their field strengths are thought to be at most 10^{8-9} Gauss). It is unclear how the external magnetic field translates into a crustal field. However, it is possible that the field strength in the crust of J1748 is higher than that in the other sources. In addition, the configuration of the field could also be quite different. Therefore, the field strength and its configuration in the crust of J1748 could be such that it affects the heat conductivity more strongly than in other cooling sources, causing a lower conductivity layer in J1748. Our NSCOOL model does not include the possibility of modelling different crustal magnetic field strengths and configurations so we cannot test this hypothesis. Moreover, a 2D code is necessary to accurately investigate this because a variety of crustal field strengths and configurations (which are not spherically symmetric) need to be simulated in order to determine if this hypothesis is physically possible (e.g. the required fields might be unrealistically high in order to affect the heat conductivity significantly) and, if so, under what conditions (e.g. maybe it might only be possible when assuming oddly shaped crustal field configuration that might only be present in certain positions in the crust).

Finally, the slow spin and large inferred surface field strength of J1748 compared to the other crust-cooling sources might indicate that the system only relatively recently (within the last 10^7 yr) started to accrete (e.g. Patruno et al. 2012). Therefore, it is possible that the original crust of the neutron star in this system has not completely been replaced by accreted matter. The possibility of the existence of neutron star systems with such hybrid crusts was discussed in detail by Wijnands, Degenaar & Page (2013). Degenaar et al. (2013) estimated (using the inferred long-term accretion rate of J1748) that indeed the inner neutron star crust in J1748 might still consist of original matter. Quite possibly the heating processes in and the

thermal conductivity of such a crust will differ strongly from that of a purely accreted crust and this could potentially explain why J1748 behaves differently than the other cooling sources. However, calculating the properties of such hybrid crusts is complex as they will change in time because matter keeps being accreted on the neutron star causing more and more of the crust to be replaced. Even if the results of such calculations will be available in the future, it remains difficult to determine exactly how much of the crust in J1748 is replaced and therefore which calculations have to be used to compare our cooling curve to. Recently, Chaikin, Kaminker & Yakovlev (2018) presented preliminary results on the thermal evolution of neutron stars with partly accreted crusts and also suggested that this might be applicable to J1748.

In order to determine the exact new base level and to better constrain the impurity parameters in the different crustal layers, additional observations are needed. Since the source is located in a globular cluster, currently only *Chandra* has the spatial resolution required to separate the X-ray emission of J1748 from the other cluster sources (see Fig. 1). Unfortunately, the source is already rather faint in our last *Chandra* observations and it requires long exposure times to get reasonable X-ray spectra. The 2016 July observations have a total exposure time of $\sim$130 ksec and similar exposure times are needed in future *Chandra* observations to accurately constrain the temperature (and likely longer since the source is expected to cool further resulting in a lower count rate). Furthermore, additional observations are only really constraining in >2000 d from now, so in about 5 yr. Observations performed earlier will improve the statistics of our current modelling constraints on the crustal parameters, but will not conclusively determine whether the source will cool down to a new base level or to the temperature measured pre-outburst.

REFERENCES

Bordas P. et al., 2010, Astron. Telegram, 2919, 1
Brown E. F., Cumming A., 2009, ApJ, 698, 1020
Brown E. F., Bildsten L., Rutledge R. E., 1998, ApJ, 504, L95
Cackett E. M., Wijnands R., Linares M., Miller J. M., Homan J., Lewin W. H. G., 2006, MNRAS, 372, 479
Campana S., Colpi M., Mereghetti S., Stella L., Tavani M., 1998, A&AR, 8, 279
Cash W., 1979, ApJ, 228, 939
Cavecchi Y. et al., 2011, ApJ, 740, L8
Chaikin E. A., Kaminker A. D., Yakovlev D. G., 2018, Ap&SS, 363, 209
Chamel N., Page D., Reddy S., 2013, Phys. Rev. C, 87, 035803

Chen W., Shrader C. R., Livio M., 1997, ApJ, 491, 312

Colpi M., Geppert U., Page D., Possenti A., 2001, ApJ, 548, L175

Cumming A., Macbeth J., in 't Zand J. J. M., Page D., 2006, ApJ, 646, 429

Cumming A., Brown E. F., Fattoyev F. J., Horowitz C. J., Page D., Reddy S., 2017, Phys. Rev. C, 95, 025806

Degenaar N. et al., 2011a, MNRAS, 412, 1409

Degenaar N. et al., 2013, ApJ, 775, 48

Degenaar N. et al., 2015, MNRAS, 451, 2071

Degenaar N., Wijnands R., 2011a, MNRAS, 412, L68

Degenaar N., Wijnands R., 2011b, MNRAS, 414, L50

Degenaar N., Wijnands R., 2012, MNRAS, 422, 581

Degenaar N., Brown E. F., Wijnands R., 2011b, MNRAS, 418, L152

Deibel A., Cumming A., Brown E. F., Page D., 2015, ApJ, 809, L31

Deibel A., Cumming A., Brown E. F., Reddy S., 2017, ApJ, 839, 95

Foreman-Mackey D., Hogg D. W., Lang D., Goodman J., 2013, PASP, 125, 306

Galloway D. K., Lin J., Chakrabarty D., Hartman J. M., 2010, ApJ, 711, L148

Garmire G. P., Bautz M. W., Ford P. G., Nousek J. A., Ricker G. R., 2003, Proc. SPIE, 4851, 28

Haensel P., Zdunik J. L., 1990, A&A, 227, 431

Haensel P., Zdunik J. L., 2008, A&A, 480, 459

Heinke C. O. et al., 2010, ApJ, 714, 894

Heinke C. O., Rybicki G. B., Narayan R., Grindlay J. E., 2006a, ApJ, 644, 1090

Heinke C. O., Wijnands R., Cohn H. N., Lugger P. M., Grindlay J. E., Pooley D., Lewin W. H. G., 2006b, ApJ, 651, 1098

Homan J., Fridriksson J. K., Wijnands R., Cackett E. M., Degenaar N., Linares M., Lin D., Remillard R. A., 2014, ApJ, 795, 131

Horowitz C. J., Berry D. K., Briggs C. M., Caplan M. E., Cumming A., Schneider A. S., 2015, Phys. Rev. Lett., 114, 031102

in 't Zand J. J. M., Homan J., Keek L., Palmer D. M., 2012, A&A, 547, A47

Lasota J.-P., 2001, New A Rev., 45, 449

Lau R. et al., 2018, ApJ, 859, 62

Linares M., Altamirano D., 2010, Astron. Telegram, 2920, 1

Mata Sánchez D., Charles P. A., Armas Padilla M., Buckley D. A. H., Israel G. L., Linares M., Muñoz-Darias T., 2017, MNRAS, 468, 564

Matsuoka M. et al., 2009, PASJ, 61, 999

Merritt R. L. et al., 2016, ApJ, 833, 186

Miller J. M., Maitra D., Cackett E. M., Bhattacharyya S., Strohmayer T. E., 2011, ApJ, 731, L7

Ootes L. S., Page D., Wijnands R., Degenaar N., 2016, MNRAS, 461, 4400

Ootes L. S., Wijnands R., Page D., Degenaar N., 2018, MNRAS, 477, 2900

Ortolani S., Barbuy B., Bica E., Zoccali M., Renzini A., 2007, A&A, 470, 1043

Page D., 2016, NSCool: Neutron star cooling code, Astrophysics Source Code Library. record ascl:1609.009

Page D., Reddy S., 2013, Phys. Rev. Lett., 111, 241102

Page D., Lattimer J. M., Prakash M., Steiner A. W., 2004, ApJS, 155, 623

Page D., Ootes L. S. , Wijnands R., Degenaar N., 2019, in press

Papitto A. et al., 2012, MNRAS, 423, 1178

Papitto A., D'Aì A., Motta S., Riggio A., Burderi L., di Salvo T., Belloni T., Iaria R., 2011, A&A, 526, L3

Parikh A. S. et al., 2017, ApJ, 851, L28

Parikh A. S. et al., 2019, A&A, 624, A84

Parikh A. S., Wijnands R., Degenaar N., Ootes L., Page D., 2018, MNRAS, 476, 2230

Patruno A., Alpar M. A., van der Klis M., van den Heuvel E. P. J., 2012, ApJ, 752, 33

Pooley D., Homan J., Heinke C., Linares M., Altamirano D., Lewin W., 2010, Astron. Telegram, 2974,, 1

Remillard R. A., 1999, Mem. Soc. Astron. Ital., 70, 881

Roggero A., Reddy S., 2016, Phys. Rev. C, 94, 015803

Rutledge R. E., Bildsten L., Brown E. F., Pavlov G. G., Zavlin V. E., Ushomirsky G., 2002, ApJ, 580, 413

Schatz H. et al., 2001, Nucl. Phys. A, 688, 150

Shternin P. S., Yakovlev D. G., Haensel P., Potekhin A. Y., 2007, MNRAS, 382, L43

Smith D. A., Morgan E. H., Bradt H., 1997, ApJ, 479, L137

Sokal A., 1997, in DeWitt-Morette C., Cartier P., Folacci A., eds, NATO ASI Series (Series B: Physics), Vol. 361, Functional Integration. Springer, Boston, MA

Steiner A. W., 2012, Phys. Rev. C, 85, 055804

Strohmayer T. E., Markwardt C. B., 2010, Astron. Telegram, 2929,, 1

Strohmayer T. E., Markwardt C. B., Pereira D., Smith E. A., 2010, Astron. Telegram, 2946,, 1

Testa V. et al., 2012, A&A, 547, A28

Turlione A., Aguilera D. N., Pons J. A., 2015, A&A, 577, A5

Ushomirsky G., Rutledge R. E., 2001, MNRAS, 325, 1157

Verner D. A., Ferland G. J., Korista K. T., Yakovlev D. G., 1996, ApJ, 465, 487

Waterhouse A. C., Degenaar N., Wijnands R., Brown E. F., Miller J. M., Altamirano D., Linares M., 2016, MNRAS, 456, 4001

Wijnands R., Strohmayer T., Franco L. M., 2001a, ApJ, 549, L71

Wijnands R., Miller J. M., Markwardt C., Lewin W. H. G., van der Klis M., 2001b, ApJ, 560, L159

Wijnands R., Guainazzi M., van der Klis M., Méndez M., 2002, ApJ, 573, L45

Wijnands R., Heinke C. O., Pooley D., Edmonds P. D., Lewin W. H. G., Grindlay J. E., Jonker P. G., Miller J. M., 2005, ApJ, 618, 883

Wijnands R., Rol E., Cackett E., Starling R. L. C., Remillard R. A., 2009, MNRAS, 393, 126

Wijnands R., Degenaar N., Page D., 2013, MNRAS, 432, 2366

Wijnands R., Degenaar N., Page D., 2017, JA&A, 38, 49

Wijngaarden M. J. P., Wijnands R., Ootes L. S., Parikh A. S., Page D., 2018, in Weltevrede P., Perera B. B. P., Preston L. L., Sanidas S., eds, IAU Symp. Vol. 337, Pulsar Astrophysics the Next Fifty Years. Kluwer, Dordrecht, p. 229 preprint (arXiv:1712.02272)

Wilms J., Allen A., McCray R., 2000, ApJ, 542, 914

Yan Z., Yu W., 2015, ApJ, 805, 87

Zhang W., Jahoda K., Kelley R. L., Strohmayer T. E., Swank J. H., Zhang S. N., 1998, ApJ, 495, L9

APPENDIX A: RESULTS OF OBSERVATIONAL ANALYSIS ASSUMING DIFFERENT MASSES AND RADII

In this section, we present the results of the reanalysis of the observations for different assumed neutron star masses and radii. We reanalysed the spectral data assuming nine different mass-radius combinations. We assumed masses of 1.0, 1.4, and 1.8 $M_\odot$, corresponding to light, intermediate, and heavy neutron stars, and radii of 10, 12, and 15 km. The resulting mass-radius combinations lead to stars that vary strongly in compactness and crust radius (see Table A2).

We reanalysed the observations in the same way as described in Section 2. The only difference is that we assumed for all spectral fits presented in this section a hydrogen column density $N_H = (3.07 \pm 0.07) \times 10^{22} \mathrm{cm}^{-2}$. For each mass-radius combination the N_H was determined from an NSATMOS fit using all spectra. The assumed N_H is the average of these values. Assuming a constant N_H throughout the spectral fits assures that the variation in resulting surface temperatures is only caused by a difference in assumed mass and radius. The obtained temperatures are presented in Table A1. In the MCMC simulations, we use linear interpolation from this grid (see Fig. A1 for the surfaces, which are almost planar, formed by the temperatures of one observation as function of mass and radius) to obtain the temperatures for any specific mass-radius combination.

Table A1. Quiescent temperatures obtained from spectral analysis for nine different assumed mass-radius combinations. The assumed neutral hydrogen column density for all spectral fits is $N_H = 3.07 \pm 0.07 \times 10^{22} \mathrm{cm}^{-2}$.

| | $kT_{\mathrm{eff}}^{\infty}$ (eV) | | | | | | | | |
| | $M = 1.0\,M_{\odot}$ | | | $M = 1.4\,M_{\odot}$ | | | $M = 1.8\,M_{\odot}$ | | |
MJD	$R = 9$ km	$R = 12$ km	$R = 15$ km	$R = 9$ km	$R = 12$ km	$R = 15$ km	$R = 9$ km	$R = 12$ km	$R = 15$ km
52833.6/55027	82.7 ± 2.0	77.6 ± 1.9	74.1 ± 1.7	80.1 ± 1.9	75.9 ± 1.8	72.5 ± 1.6	77.2 ± 1.8	74.2 ± 1.8	71.1 ± 1.7
55609.4	115.3 ± 1.7	107.9 ± 1.5	102.2 ± 1.4	111.4 ± 1.6	105.0 ± 1.4	100.1 ± 1.4	107.0 ± 1.5	102.2 ± 1.4	98.0 ± 1.3
55680.7	104.4 ± 1.7	98.0 ± 1.6	93.0 ± 1.5	100.7 ± 1.6	95.5 ± 1.5	91.1 ± 1.4	97.0 ± 1.6	93.1 ± 1.4	89.4 ± 1.4
55812.7	102.8 ± 1.6	96.4 ± 1.5	91.4 ± 1.4	99.1 ± 1.6	94.0 ± 1.5	89.6 ± 1.4	95.4 ± 1.5	91.6 ± 1.4	87.8 ± 1.4
56060.8	96.3 ± 1.9	90.5 ± 1.7	86.1 ± 1.6	93.0 ± 1.8	88.4 ± 1.7	84.4 ± 1.6	89.5 ± 1.8	86.3 ± 1.6	82.9 ± 1.5
56207.9	98.5 ± 1.6	92.5 ± 1.5	87.8 ± 1.4	95.0 ± 1.5	90.2 ± 1.4	86.1 ± 1.4	91.5 ± 1.5	88.0 ± 1.4	84.5 ± 1.3
56336.8	95.3 ± 0.9	89.5 ± 0.9	84.9 ± 0.8	92.1 ± 0.9	87.3 ± 0.9	83.2 ± 0.8	88.5 ± 0.9	85.1 ± 0.8	81.6 ± 0.8
56489.9	96.9 ± 2.4	91.0 ± 2.2	86.6 ± 2.1	93.6 ± 2.2	88.9 ± 2.1	84.9 ± 2.0	90.0 ± 2.2	86.7 ± 2.0	83.3 ± 2.0
56855.8	94.2 ± 1.4	88.0 ± 1.3	83.3 ± 1.2	90.8 ± 1.3	85.9 ± 1.2	81.7 ± 1.2	87.0 ± 1.2	83.7 ± 1.2	80.1 ± 1.1
57583.6	90.3 ± 1.3	84.5 ± 1.2	80.0 ± 1.2	87.2 ± 1.3	82.4 ± 1.2	78.5 ± 1.1	83.7 ± 1.2	80.4 ± 1.1	77.0 ± 1.1

Table A2. Overview of the surface gravity and crust radius for the nine different mass-radius combinations for which the observational data were reanalysed.

| | $R = 9$ km | | $R = 12$ km | | $R = 15$ km | |
M ($M_{\odot}$)	g_s (10^{14} cm s^{-2})	ΔR (km)	g_s (10^{14} cm s^{-2})	ΔR (km)	g_s (10^{14} cm s^{-2})	ΔR (km)
1.0	2.00	0.96	1.06	1.83	0.66	2.93
1.4	3.12	0.58	1.59	1.20	0.97	2.01
1.8	4.61	0.35	2.22	0.81	1.32	1.43
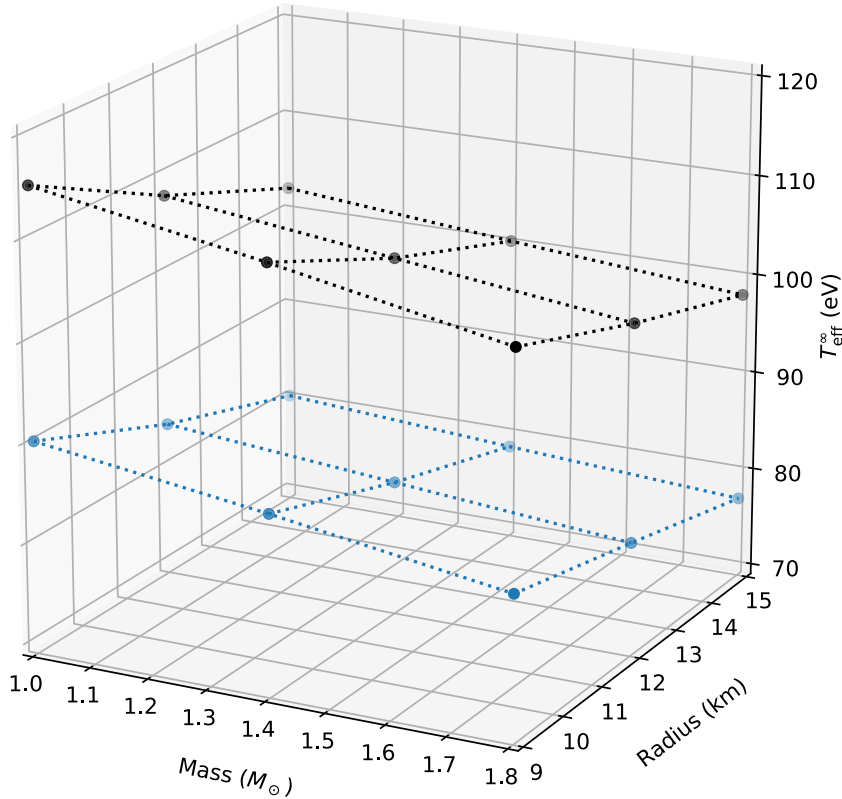
Figure A1. 3-dimensional representation of the temperatures of the first (black points) and last (blue points) observation for different assumed masses and radii. The surfaces formed by the temperatures of intermediate observations are omitted for clarity.
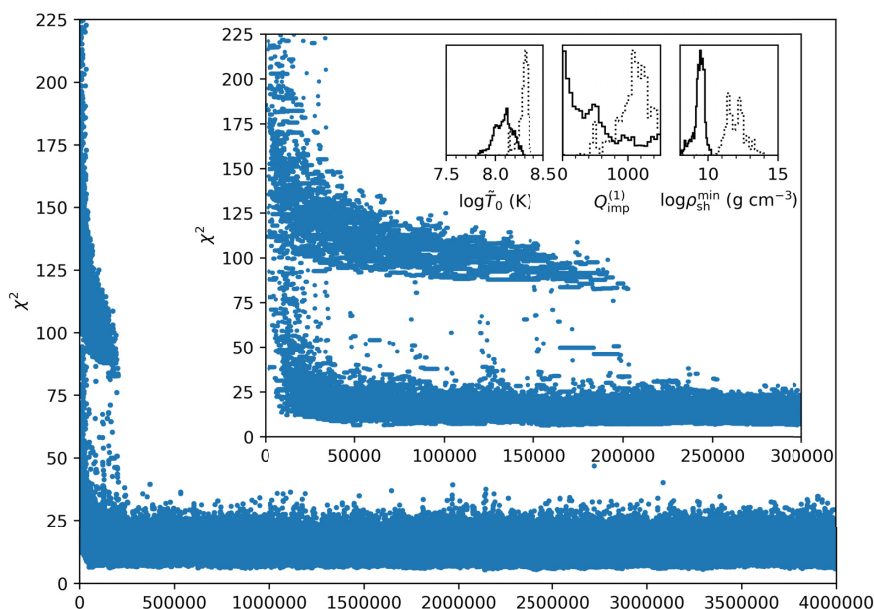
APPENDIX B: ADDITIONAL FIGURES OF MCMC SIMULATIONS

Figure B1. Scatter plot of χ^2 in our model 2 run showing a short initial burn-in phase of $\sim$30 000 points during which all χ^2 drop below 200, but exhibiting part of the walkers trapped in a local minimum with $\chi^2 > 75$ till more than 200 000 points have been generated. The inset shows the first 300 000 points in more detail and within it histograms of T_0, $Q_{imp}^{(1)}$, and $\log \rho_{sh, min}$ from the points 50 000–200 000 with $\chi^2 < 75$ as continuous lines and with $\chi^2 > 75$ as doted lines clearly exhibiting the bi-modality. This *seems* to indicate that after about 300 000 points the chain has converged, but the next figure shows that this likely required 1 000 000 points.
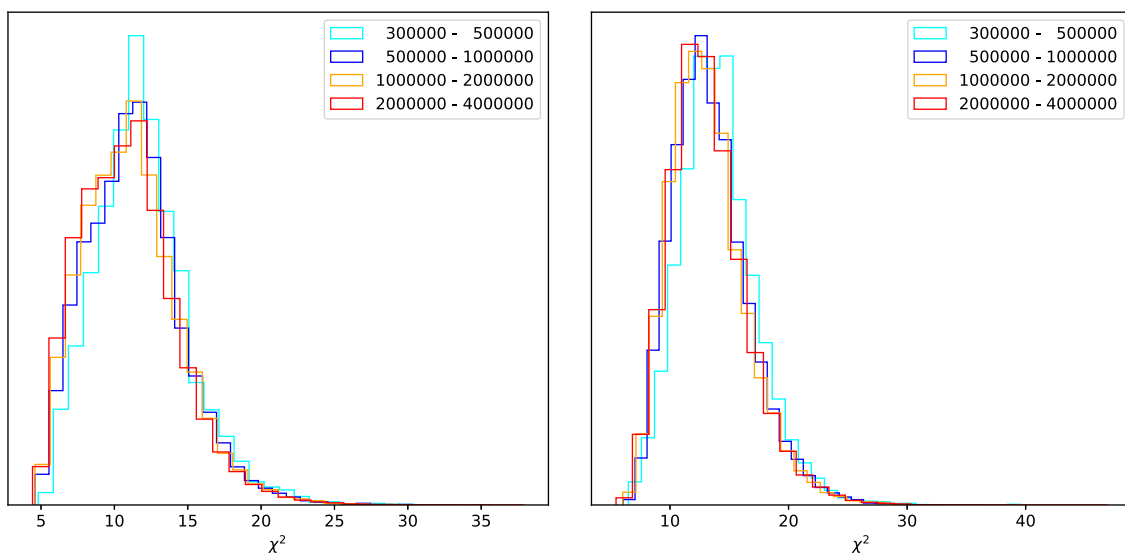

Figure B2. The χ^2 distributions for selected number points in our MCMC run for model 1 (left) and model 2 (right). As there seems to be no significant change in the distributions after 1 million points (for both panels), we concluded that convergence seemed to be reached at that stage. We therefore eliminated the initial 1 million curves as 'burn-in phase' from our total of 4 million cooling curves.

This paper has been typeset from a TEX/LATEX file prepared by the author.